

Successive magnetic transitions in heavy fermion superconductor $\text{Ce}_3\text{PtIn}_{11}$ studied by ^{115}In nuclear quadrupole resonance

Hideto Fukazawa ^{*1}, Kazuki Kumeda¹, Naoki Shioda¹, Yongsun Lee¹, Yoh Kohori¹, Koudai Sugimoto², Debarchan Das^{3,4}, Joanna Bławat³ and Dariusz Kaczorowski³

¹*Department of Physics, Chiba University, Chiba 263-8522, Japan*

²*Department of Physics, Keio University, Yokohama 223-8522, Japan*

³*Institute of Low Temperature and Structure Research,*

Polish Academy of Sciences, P.O. Box 1410, PL-50-950 Wrocław, Poland

⁴*Laboratory for Muon Spin Spectroscopy, Paul Scherrer Institute, CH-5232 Villigen PSI, Switzerland*

(Dated: October 13, 2020)

Nuclear quadrupole resonance (NQR) measurements were performed on the heavy fermion superconductor $\text{Ce}_3\text{PtIn}_{11}$ with $T_c = 0.32$ K. The temperature dependence of both spin-lattice relaxation rate $1/T_1$ and NQR spectra evidences the occurrence of two successive magnetic transitions with $T_{N1} \simeq 2.2$ K and $T_{N2} \simeq 2.0$ K. In successive magnetic transitions, even though the magnetic moment at the Ce(2) site plays a major role, the magnetic moment at the Ce(1) site also contributes to some extent. While a commensurate antiferromagnetic ordered state appears for $T_{N2} < T < T_{N1}$, a partially incommensurate antiferromagnetic ordered state is suggested for $T < T_{N2}$.

I. INTRODUCTION

Ce-based intermetallic systems have gained considerable research interest due to their diverse and perplexing physical properties encompassing observation of non-Fermi-liquid behavior, heavy-fermion-superconductivity, and quantum criticality [1–5]. Among the vast number of known compounds, the members of the $\text{Ce}_nM_m\text{In}_{3n+2m}$ ($M = \text{Co}, \text{Rh}, \text{Pd}, \text{Ir}, \text{Pt}$) family have drawn an unprecedented amount of research effort due to their fascinating phase diagrams, which allow exploration of the relationship between magnetism and adjacent superconductivity.

Among them, CeIn_3 ($m = 0, n = 1$) is a three-dimensional material, and the localized magnetism of Ce ions is dominant at ambient pressure ($T_N = 10$ K) [2]. However, with increasing pressure, antiferromagnetic order is gradually suppressed, the hybridization between Ce f electrons and conduction electrons becomes significant, and finally superconductivity emerges near the magnetic quantum critical point ($T_c = 0.2$ K at 2.6 GPa). In turn, the $\text{Ce}M\text{In}_5$ phases ($m = n = 1$) have quasi-two-dimensional character. CeCoIn_5 is one of the most intensively studied systems in recent times due to its unique physics associated with heavy-fermion superconductivity at ambient pressure ($T_c = 2.3$ K) and normal-state non-Fermi-liquid behavior [3, 6]. In high magnetic fields, confined in the basal plane of the tetragonal unit cell, an inhomogeneous superconducting phase of the Fulde-Ferrell-Larkin-Ovchinnikov (FFLO) type possibly forms at the lowest temperatures [7–9]. The compound CeRhIn_5 , isostructural to CeCoIn_5 , is antiferromagnetic at ambient pressure ($T_N = 3.8$ K), and exhibits superconductivity under pressure ($T_c = 2.1$ K at 2.0 GPa) [10, 11]. Maximum T_c is about an order of magnitude higher than that

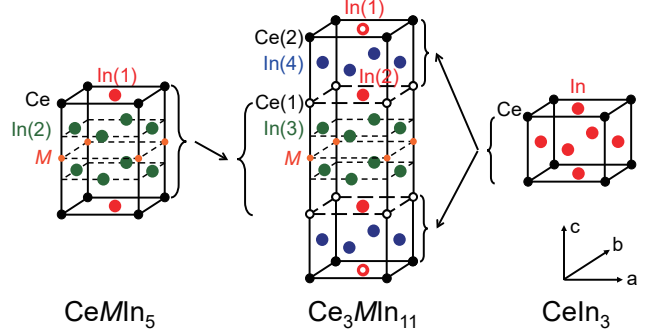


FIG. 1: Crystal structures of the $\text{Ce}_nM\text{In}_{3n+2}$ ($n = 1, 3, \infty, M = \text{Co}, \text{Rh}, \text{Pd}, \text{Ir}, \text{Pt}$) compounds. One of the principal axes of the electric field gradient V_{zz} is perpendicular to the crystal ab plane for the In(1) and In(2) sites and parallel to the a or b axis for the In(3) and In(4) sites [24, 25].

of CeIn_3 , which is a consequence of the reduced effective dimensionality [12]. Ce_2PdIn_8 ($m = 1, n = 2$) exhibits superconductivity below $T_c = 0.64$ K [13, 14]. There, the antiferromagnetic fluctuations are not as strong as in CeCoIn_5 [15, 16].

Recently, the synthesis of $\text{Ce}_3M\text{In}_{11}$ ($m = 1, n = 3$) has been reported [17, 18]. Unlike $\text{Ce}M\text{In}_5$, Ce_2MIn_8 , and CeIn_3 , in which a single Ce site exists, there are two inequivalent Ce sites in the unit cell of the $\text{Ce}_3M\text{In}_{11}$ crystal, namely, Ce(1) at the $4mm$ site and Ce(2) at the $4/mmm$ site. The structure gives a new interest in considering magnetism and superconductivity in the $\text{Ce}_nM_m\text{In}_{3n+2m}$ group. Both $\text{Ce}_3\text{PtIn}_{11}$ and $\text{Ce}_3\text{PdIn}_{11}$ exhibit two successive antiferromagnetic phase transitions at ambient pressure ($T_{N1} \simeq 2.2$ K and $T_{N2} \simeq 2.0$ K for $M = \text{Pt}$, $T_{N1} \simeq 1.7$ K and $T_{N2} \simeq 1.5$ K for $M = \text{Pd}$) [18]. Even in the antiferromagnetic state, they exhibit superconductivity below $T_c = 0.32$ K ($M = \text{Pt}$) and 0.42 K ($M = \text{Pd}$) [19, 20]. In each material, a further metamagnetic transition occurs in a high magnetic

*hideto@chiba-u.jp

field [21, 22]. This suggests that the coexistence of antiferromagnetism and superconductivity in the Ce_3MIn_{11} compounds is quite a unique phenomenon driven by the hybridization between f electrons of Ce ions and conduction electrons [23]. Naively, the superconductivity and two successive antiferromagnetic transitions can be considered to be due to two inequivalent Ce sites. The localized magnetic moment of the Ce(2) site (depicted in Fig. 1) is supposed to be responsible for the magnetic transitions. In turn, the Ce(1) site is either nonmagnetic or very weakly magnetic, as suggested by the specific heat data [18, 19]. This duality of Ce sites facilitates understanding of new physics near the quantum critical point. For this purpose, knowledge of magnetic structures in the Ce_3MIn_{11} compounds is essential. However, due to excessive In content in this system, standard neutron diffraction measurements are difficult to perform and time consuming because In has a large absorption cross section. Thus local probe measurements such as nuclear quadrupole resonance (NQR) can be of great use, and indeed such experiments have recently been performed for Ce_3PtIn_{11} by Kambe *et al.* [24, 25]. However, it must be noted that the successive magnetic transitions, which were observed by specific-heat and magnetic-susceptibility measurements, were not clearly observed in NQR [25]. The NQR data suggested that the wave vector of the magnetic structure below T_{N1} was $(\frac{1}{2}, \frac{1}{2}, h)$ with an incommensurate k_z component of the wave vector. The magnetic moment at the Ce(2) site has a main component along the crystal c axis and a tilted component within the ab plane. This magnetic structure is similar to that of $CeRhIn_5$, where the wave vector is expressed with $(\frac{1}{2}, \frac{1}{2}, 0.297)$ [26, 27]. Moreover, taking into account the decrease in signal intensity due to the internal magnetic field at each In site, Kambe *et al.* concluded that the localized moment of the Ce(2) ion gives the main contribution to the magnetically ordered state in Ce_3MIn_{11} , as suggested first in Ref. [19].

In this paper, we performed detailed measurements of the NQR spectra and the spin-lattice relaxation rate $1/T_1$ of Ce_3PtIn_{11} with a focus on the In(2), In(3), and In(4) sites. In both physical quantities, two successive transitions were clearly observed, which were not detected in the previous study [24]. From the viewpoint of the NQR spectra, each inequivalent In site has a single internal magnetic field between T_{N1} and T_{N2} , and the In(3) site feels two or more different internal magnetic fields below T_{N2} . Based on the results of our study, we suggest the most probable magnetically ordered state in Ce_3PtIn_{11} , in which a wave vector with $(\frac{1}{2}, \frac{1}{2}, 0, \text{ or } \frac{1}{2})$ is realized between T_{N1} and T_{N2} . Our analysis suggests that this wave vector changes into a commensurate or an incommensurate vector depending on the inequivalent Ce sites below T_{N2} .

II. EXPERIMENTS

A polycrystalline sample of Ce_3PtIn_{11} was obtained in a two-step procedure. First, $CeIn_2$ and Pt_3In_7 binaries were synthesized by melting the high-purity elemental constituents under a high-purity argon atmosphere using an arc furnace installed inside an MBRAUN glove box with controlled oxygen and moisture contents. Then, the two precursors were arc-melted in the same furnace together with elemental indium in the proportion 9:1:8, required to get the nominal composition Ce_3PtIn_{11} . The button was turned over and remelted several times to promote homogeneity. The final mass loss was less than 1%. The so-obtained sample was wrapped with tantalum foil and annealed in an evacuated quartz ampoule at 500°C for 4 weeks, followed by quenching in cold water. Quality of the product was checked by x-ray powder diffraction, by energy-dispersive x-ray analysis, and by bulk property measurements. The detailed synthesis process and preliminary characterization data are reported elsewhere [28]. The sample contains a partial parasitic phase of $CeIn_3$ (less than 5%-10%) but has a fairly sharp superconducting transition at $T_c \simeq 0.33$ K and two antiferromagnetic transitions at $T_{N1} = 2.2$ K and $T_{N2} = 2.0$ K, in agreement with the literature data [18, 21]. For NQR measurements, the sample was fine powdered in order to reduce the heating-up effect at low temperatures and improve the NQR signal intensity. The ^{115}In NQR studies were performed in the frequency range of 7-70 MHz using a phase-coherent pulsed NQR spectrometer. Measurements down to 1.4 K were carried out using a 4He cryostat. The spin-lattice relaxation time T_1 was obtained from the recovery of the nuclear magnetization after a saturation pulse.

III. RESULTS AND DISCUSSION

A. In-NQR spectrum at 4.2 K

Figure 2 shows the NQR spectrum of Ce_3PtIn_{11} taken at 4.2 K. The obtained data are very similar to those reported before [24, 25]. As can be inferred from Fig. 1, there are four inequivalent crystallographic positions for indium atoms in the unit cell of Ce_3PtIn_{11} , namely, In(1) ($4/mmm$), In(2) ($4mm$), In(3) ($2mm$), and In(4) ($2mm$). (We follow the notation of site index indicated by Kambe *et al.* [24, 25].) For the In nuclei ($I = 9/2$), the electric quadrupole Hamiltonian \mathcal{H}_Q is given by

$$\mathcal{H}_Q = \frac{e^2qQ}{4I(2I-1)} \left\{ 3I_z^2 - I(I+1) + \frac{\eta}{2}(I_+^2 + I_-^2) \right\}, \quad (1)$$

where eq , eQ , and η represent the electric field gradient (EFG), the nuclear quadrupole moment, and the asymmetry parameter of the EFG, respectively. η is defined by $\frac{V_{xx} - V_{yy}}{V_{zz}}$, where V_{xx} , V_{yy} , and V_{zz} are the principal

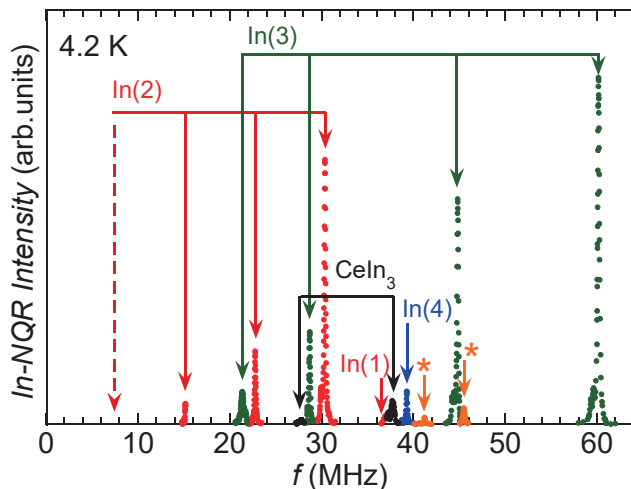


FIG. 2: In-NQR spectrum of $\text{Ce}_3\text{PtIn}_{11}$ at 4.2 K. Signal indicated by * is of parasitic phase.

axes of the EFG and $|V_{zz}| \geq |V_{yy}| \geq |V_{xx}|$. By diagonalizing \mathcal{H}_Q and considering the four inequivalent In sites in $\text{Ce}_3\text{PtIn}_{11}$, one can assign all the observed features in the NQR spectrum. For each In site, four resonance lines appear with increasing frequencies: ν_1 , ν_2 , ν_3 , and ν_4 . The ν_1 line corresponds to the transition between $|I_z = \pm 1/2\rangle$ and $|I_z = \pm 3/2\rangle$, the ν_2 line is due to the transition between $|I_z = \pm 3/2\rangle$ and $|I_z = \pm 5/2\rangle$, etc. Note that ν_1 differs from the resonance frequency $\nu_Q \equiv \frac{3e^2qQ}{2I(2I-1)}$ except for the case of $\eta = 0$. For sites with $\eta = 0$, they are equidistant, and for those with $\eta \neq 0$, they are not equidistant. Therefore, for the In(2) [or In(1)] site, it can be determined as a site with $\eta = 0$ without numerical calculation. However, for other sites, it is necessary to perform numerical calculation to identify the site.

The obtained NQR frequency ν_Q and the parameter η are 7.591(2) MHz and 0.000(1), respectively, for In(2), and 15.114(4) MHz and 0.2388(4), respectively, for In(3). We also observed the NQR signals at the positions that were assigned before (see above) as ν_4 lines of In(1) and In(4) [24, 25]. Therefore the NQR spectrum obtained at 4.2 K is consistent with that previously obtained at 3.1 K in the paramagnetic state.

As shown in Fig. 2, some weak NQR signals were attributable to antiferromagnetically-ordered CeIn_3 . In addition, we found two extra lines at around 41.2 and 45.5 MHz, which could be assigned to neither $\text{Ce}_3\text{PtIn}_{11}$ nor CeIn_3 and hence likely arise due to other parasitic phases, which were also pointed out previously [24, 25].

B. In-NQR spectra between 1.4 and 4.2 K

We followed the temperature evolution of the ν_2 to ν_4 lines of the In(2) site, all lines of the In(3) site, and the ν_4 line of the In(4) site. In the spectrum recorded at 4.2 K, the ν_4 line of the In(1) site had quite a short spin-

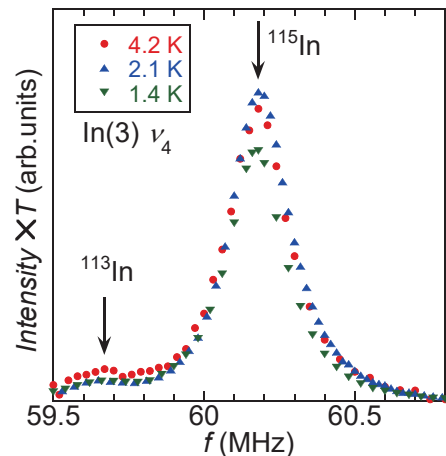


FIG. 3: In-NQR spectra of $\text{Ce}_3\text{PtIn}_{11}$ for ν_4 lines of the In(3) site at 1.4, 2.1, and 4.2 K. These spectra are multiplied by temperature and are corrected for the effect of spin-spin relaxation time T_2 .

relaxation time T_2 . If T_2 is long enough, the NQR signal intensity simply increases in inverse proportion to the temperature, but if T_2 becomes short around T_N , its correction must be taken into account [30]. Just for this reason, we could not follow the ν_4 line of the In(1) site below T_{N1} . Figure 3 shows the spectra of the ν_4 line at the In(3) site at 1.8, 2.1, and 4.2 K. These spectra were multiplied by temperature and T_2 corrected. The spectral line of ^{113}In nuclei is observed on the lower-frequency side of the ^{115}In line [31]. Regarding the ν_2 , ν_3 , and ν_4 lines of the In(2) site as well as the ν_3 line of the In(3) site, the spectra were almost independent of temperature, similarly to the ν_4 line of the In(3) site. On the other hand, the ν_1 and ν_2 lines of the In(3) site and the ν_4 line of the In(4) site showed a clear change in the spectrum taken below T_{N1} .

Figure 4 shows the temperature evolution of the ν_2 line of the In(3) site. These spectra were also multiplied by temperature and T_2 corrected. At 4.2 K, we observed a narrow NQR line. In addition, a signal from a parasitic phase, as small as that of ^{113}In nuclei, was also observed on the lower-frequency side of the ^{115}In line [31]. Notably, with decreasing temperature, the feature splits into two lines in the temperature region between 2.0 and 2.2 K (labeled L1 in Fig. 4). The spectra below 2.0 K are more complicated. Around the center of the spectra, the separation of lines decreases with decreasing temperature, and the two lines merge into a single line below 1.8 K (L2 in Fig. 4). Below 2.0 K, another couple of separated lines appear outside the original separated lines (L3 in Fig. 4). The spectrum changes continuously through $T = T_{N2}$. Therefore the phase transition at T_{N2} cannot be interpreted as a phase separation of the paramagnetic phase and the antiferromagnetically ordered phase.

Figure 5 shows the temperature evolution of the ν_4

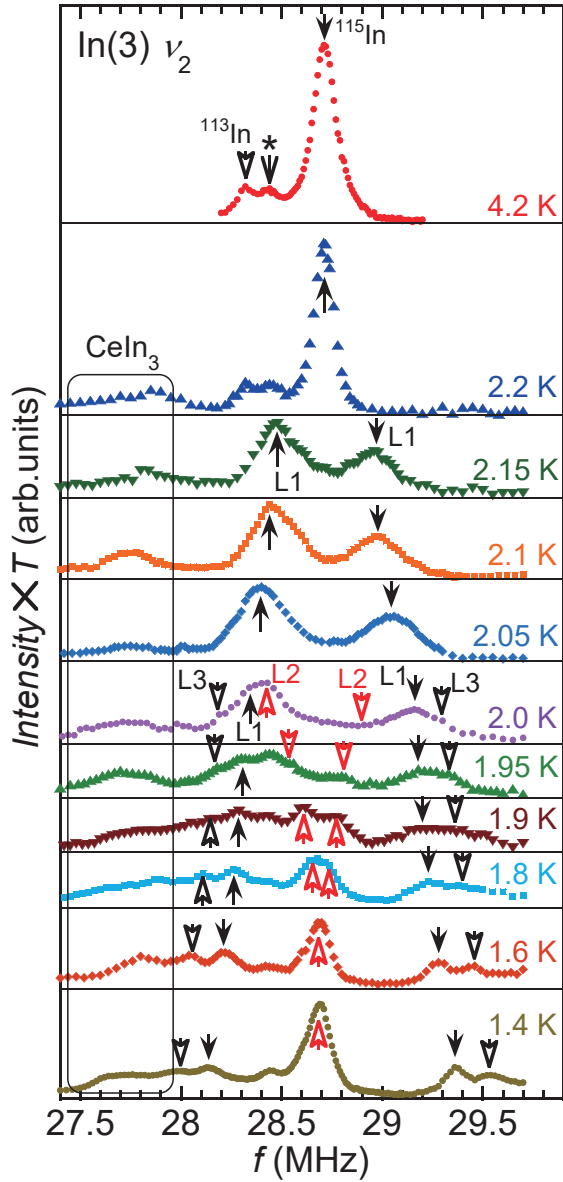


FIG. 4: The temperature evolution of the In-NQR spectrum of $\text{Ce}_3\text{PtIn}_{11}$ for the ν_2 lines of the In(3) site. Signal indicated by * is of parasitic phase. The characteristic structure observed in the spectra is indicated by several kinds of arrows (L1, L2, and L3).

spectrum of the In(4) site. The experimental results were T_2 corrected only for the data obtained at 2.2 and 4.2 K. This is because the signal intensity decreased considerably below T_{N1} , which hampered precise evaluation of T_2 . The recovery of the signal at 1.5 K is probably due to increase of T_2 below T_{N2} . Unlike lines of the In(3) site, the ν_4 line of the In(4) site shifts monotonically to the low-frequency side without any splitting below T_{N1} . The peak of the spectrum at 1.5 K is around 38.7 MHz, which is consistent with the previous reports [24, 25].

In order to determine the direction of the internal mag-

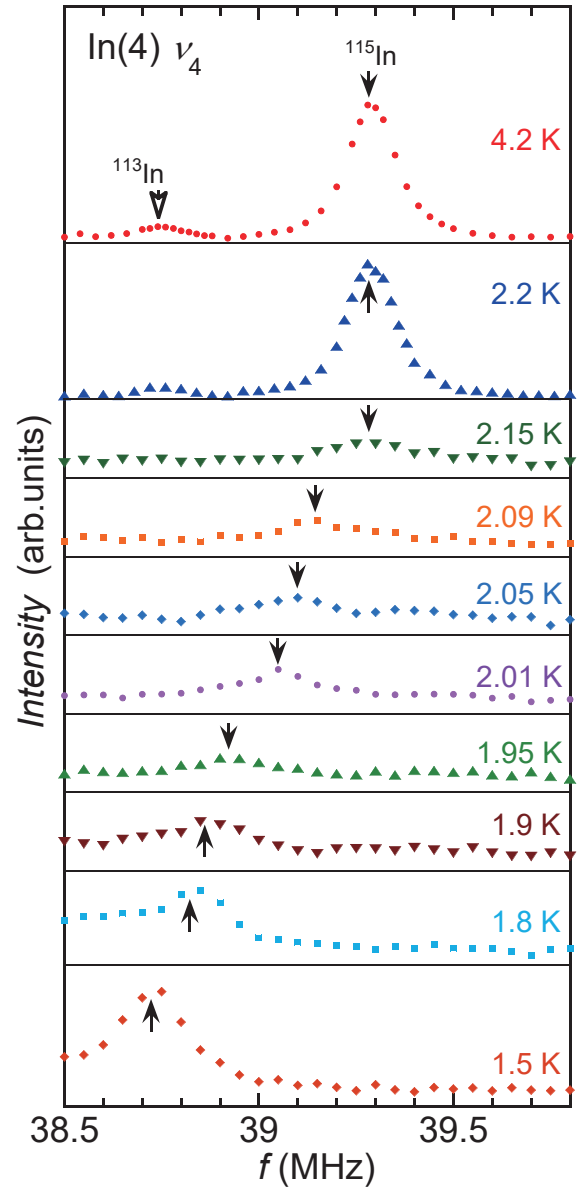


FIG. 5: The temperature evolution of the In-NQR spectrum of $\text{Ce}_3\text{PtIn}_{11}$ for the ν_4 line of the In(4) site. The effect of T_2 was taken into account only for the data obtained at 2.2 and 4.2 K.

netic field and evaluate the contribution of the internal magnetic field at the In(2), In(3), and In(4) sites, we added to the Hamiltonian described in Eq. (1) the following Zeeman-effect Hamiltonian:

$$\begin{aligned} \mathcal{H}_Z &= -\mu_N \vec{I} \cdot \vec{B}_{\text{int}} \\ &= -\mu_N B_{\text{int}} (I_x \sin \theta \cos \varphi + I_y \sin \theta \sin \varphi + I_z \cos \theta), \end{aligned} \quad (2)$$

where μ_N , B_{int} , θ , and φ are the nuclear magneton of indium, the internal magnetic field at the In sites, the polar angle from V_{zz} , and the azimuthal angle from V_{xx} , respectively.

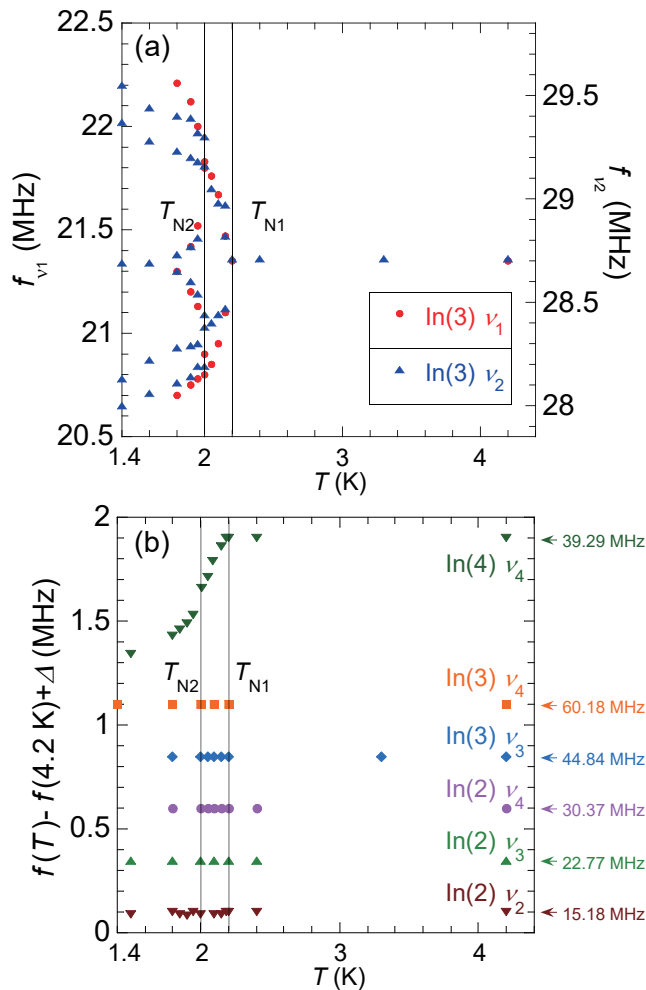


FIG. 6: Temperature dependence of the characteristic frequencies in the spectra of $\text{Ce}_3\text{PtIn}_{11}$ for (a) the ν_1 and ν_2 lines of the In(3) site and (b) the ν_2 , ν_3 , and ν_4 lines of the In(2) site, the ν_3 and ν_4 lines of the In(3) site, and the ν_4 line of the In(4) site. For the latter case, $f(T) - f(4.2 \text{ K})$ is properly shifted so that the lines do not overlap with each other.

Figure 6 shows the temperature dependence of the characteristic frequencies of each line measured for $\text{Ce}_3\text{PtIn}_{11}$. First, the ν_2 , ν_3 , and ν_4 lines of the In(2) site are nearly independent of temperature [see Fig. 6(b)]. This feature clearly implies that the internal magnetic field is canceled out at this site. Next, it can be seen that both ν_1 and ν_2 of the In(3) site show almost the same and clear temperature dependences [see Fig. 6(a)]. This is in contrast to the fact that both ν_3 and ν_4 of the In(3) site do not change through out the entire temperature range. These results indicate that, at the In(3) site, the internal field broadens the ν_1 and ν_2 lines, yet does not affect the ν_3 and ν_4 lines. Performing numerical calculations in terms of Eqs. (1) and (2), one can easily deduce that $\theta = \frac{\pi}{2}$ is realized in the ordered state. Moreover, the numerical diagonalization of the Hamiltonians reveals that $\varphi = \frac{\pi}{2}$ is more likely rather than $\varphi = 0$. The

calculation revealed that a range $\frac{\pi}{3} \lesssim \varphi \leq \frac{\pi}{2}$ is allowed to account for the data because of the finite asymmetry parameter η at the In(3) site. Following this finding, the value of the internal magnetic field of 25 mT was found, which can explain the spectral splitting of the In(3) site at T_{N2} . Finally, the peak frequency of the ν_4 line of the In(4) site decreases monotonically without splitting below T_{N1} . This requires at least $\theta = \frac{\pi}{2}$, which implies that the direction of the internal magnetic field at the In(4) site is the same as or close to that at the In(3) site. Therefore the internal magnetic field can be evaluated from the shift of the ν_4 line of the In(4) site. At T_{N2} , such a shift attains about 0.3 MHz, which corresponds to an internal magnetic field of about 400 mT.

C. Dipolar model analysis

Here, we consider the magnetic moments at the Ce sites and the wave vectors, which correspond to the obtained direction and magnitude of the internal magnetic fields at T_{N2} based on the appearance of the antiferromagnetic order in $\text{Ce}_3\text{PtIn}_{11}$. We assume the wave vector of $(\frac{1}{2}, \frac{1}{2})$ in the k_x - k_y plane of the wave vector space; by analogy to other $\text{Ce}_n\text{M}_m\text{In}_{3n+2m}$ compounds, $k = (\frac{1}{2}, \frac{1}{2}, 0)$ for Ce_2RhIn_8 , $(\frac{1}{2}, \frac{1}{2}, \frac{1}{2})$ for CeIn_3 [32] and CePt_2In_7 [33–36], and $(\frac{1}{2}, \frac{1}{2}, 0.297)$ for CeRhIn_5 [26, 27]. Most importantly, a similar wave vector $(\frac{1}{2}, \frac{1}{2}, h)$ was recently also suggested for $\text{Ce}_3\text{PtIn}_{11}$ [25]. Based on the latter finding, we set the moment at the Ce (2) site as $\vec{m} = (m_a, m_b, m_c)$ and assume that the Ce(1) site is non-magnetic or very weakly magnetic. Then, the internal magnetic fields at the In(1) and In(2) sites are roughly proportional to $(m_b, m_a, 0)$, while those at the In(3) and In(4) sites are proportional to $(0, m_c, m_b)$, if one of the principal axes of the EFG (V_{zz}) is parallel to the crystal a axis for which the In(3) and In(4) sites are located in the crystal bc plane [or $(m_c, 0, m_a)$ if V_{zz} is parallel to the b axis for which the In(3) and In(4) sites are located in the ac plane].

First, since the internal magnetic field does not appear at the In(2) site below T_{N1} , the ordered magnetic moment has only a c -axis component ($m_a = m_b = 0$). Kambe *et al.* [24, 25] pointed out that the disappearance of the signal at the In(1) site implies the appearance of an internal magnetic field parallel to the principal axis V_{zz} of the EFG. In such a case, a similar clear internal magnetic field would have appeared at the In(2) site, and all the In(2) lines must split, which is inconsistent with our experimental results. Therefore it is reasonable to presume that the extremely short relaxation time T_2 makes difficult observation of the signal at the In(1) site below T_{N1} . In addition, Kambe *et al.* [24, 25] suggested some possibility of a wave vector of $(0, 0, \frac{1}{2})$ with a magnetic moment direction along the c axis. However, in such a case, a large internal magnetic field would have also appeared at the In(2) site. Hence this conjecture must be ruled out.

TABLE I: $\nu_Q(\text{calc})$ and $\eta(\text{calc})$ are calculated based on the electronic structure calculation using the WIEN2K code [29]. $\nu_Q(\text{exp})$ and $\eta(\text{exp})$ are experimentally obtained at 4.2 K.

	$\nu_Q(\text{calc})$ (MHz)	$\eta(\text{calc})$	$\nu_Q(\text{exp})$ (MHz)	$\eta(\text{exp})$
In(1)	10.1	0	(9.24)	
In(2)	8.73	0	7.591(2)	0.000(1)
In(3)	14.5	0.190	15.114(4)	0.2388(4)
In(4)	10.4	0.00054	(~ 9.8)	

Next, in the case that V_{zz} is parallel to the crystal a axis [the In(3) sites located in the bc plane], an internal magnetic field parallel to $(0, m_c, 0)$ should appear at the In(3) site because the in-plane component of the magnetic moment must be zero ($m_a = m_b = 0$: see the discussion above). In order to confirm the relation between the principal axes of the EFG and the crystal axes, we performed the electronic structure calculation using the WIEN2K code [29], where the full-potential linearized augmented-plane-wave method with the generalized gradient approximation for electron correlations is used. For calculations, the space group, the lattice constants, and the starting positions of atoms in the cell were taken from Tables I and II of Ref. [21], and the positions of the atoms were finally determined by structure optimizations. For comparison, Table I summarizes the calculated and the experimentally determined ν_Q and η . Both values are consistent with each other, which ensures the reliability of the calculations. The calculated values of V_{aa} , V_{bb} , and V_{cc} , before the rotation of the principal axes, are 17.75, -10.56, and -7.19, respectively in units of 10^{21} V/m². These values were calculated for the In(3) sites located in the crystal bc plane. Hence this means that V_{xx} , V_{yy} , and V_{zz} , after the rotation of the principal axes, are parallel to the c axis, b axis and a axis, respectively, which implies that the internal magnetic field at the In(3) site is perpendicular to both V_{zz} and V_{xx} . This is consistent with the experimentally obtained direction of the internal magnetic field at the In(3) site ($\theta = \frac{\pi}{2}$, $\frac{\pi}{3} \lesssim \varphi \leq \frac{\pi}{2}$). At least between T_{N1} and T_{N2} , the In(3) site feels a homogeneous internal magnetic field of $\simeq 25$ mT. Otherwise, the spectrum would be much broader and the obtained values of the internal magnetic fields would also be distributed. This adds a condition that the wave number along the k_z direction must be commensurate. Accordingly, the wave vector should be either $(\frac{1}{2}, \frac{1}{2}, 0)$ or $(\frac{1}{2}, \frac{1}{2}, \frac{1}{2})$, and the magnetic moment must be parallel to the c axis between T_{N1} and T_{N2} . This conclusion is different from the suggestion by the previous report that required inclination of the magnetic moment from the c axis [25].

TABLE II: Antiferromagnetic wave vectors, magnetic moments, and the dipole field sum at the In(3) and In(4) sites for the experimental internal magnetic fields of the In(3) and In(4) sites at T_{N2} . Calculations were performed for the In(3) and In(4) sites located in the crystal bc plane.

	Wave vector	m/μ_B	$\vec{B}_{\text{In}(3)}$ (mT)	$\vec{B}_{\text{In}(4)}$ (mT)
Ce(1)	$(\frac{1}{2}, \frac{1}{2}, 0)$	0.20	(0, 15.4, 0)	(0, -15.4, 0)
Ce(2)	$(\frac{1}{2}, \frac{1}{2}, 0)$	5.30	(0, 9.2, 0)	(0, 416.7, 0)
(Total)			(0, 24.6, 0)	(0, 401.3, 0)
Ce(1)	$(\frac{1}{2}, \frac{1}{2}, \frac{1}{2})$	0.19	(0, 15.3, 0)	(0, -14.6, 0)
Ce(2)	$(\frac{1}{2}, \frac{1}{2}, \frac{1}{2})$	5.29	(0, 9.6, 0)	(0, 415.9, 0)
(Total)			(0, 24.9, 0)	(0, 401.3, 0)

By calculating the dipole magnetic field with $(\frac{1}{2}, \frac{1}{2}, 0)$ or $(\frac{1}{2}, \frac{1}{2}, \frac{1}{2})$, we have checked whether the experimentally obtained internal magnetic fields at T_{N2} could be reproduced, i.e., 25 mT at the In(3) site and 400 mT at the In(4) site. For the numerical calculations of the dipole field with the magnetic moment along the crystal c axis, $120 \times 120 \times 30$ unit cells were used, and it was confirmed that the calculations converged by the calculation radius of about 10 nm. Here, we used the structure data (space group, lattice constants, and positions of atoms) summarized in Tables I and II of Ref. [21]. First, we assumed the magnetic moment only at the Ce(2) site. However, in this case, we were not able to determine the size of the magnetic moment that could explain the internal magnetic fields at both In sites [37]. Next, we additionally assumed the magnetic moment at the Ce(1) site. For simplification, we set the magnetic moment of the Ce(1) site parallel to that of the Ce(2) site belonging to the same unit cell. Then, we obtained the set of the magnetic moments summarized in Table II, which is consistent with the experimentally obtained internal magnetic fields. The contribution of the internal magnetic field at the In(3) site is attributable to the magnetic moments of the Ce(1) and Ce(2) sites. On the other hand, the main contribution of the field at the In(4) site is ascribable to the moment of the Ce(2) site. Remarkably, the moment of the Ce(1) site is about 4% of that of the Ce(2) site in both cases. This indicates that the magnetic moment of the Ce(1) site is very small and that the magnetic moment of the Ce(2) site plays a main role in the magnetism of $\text{Ce}_3\text{PtIn}_{11}$. The evaluated moment for the Ce(2) site is much larger than $g_J = 15/7 \simeq 2.14 \mu_B$ expected for the Ce^{3+} ion. In the actual system, each In site feels a pseudo-dipole field transferred by conduction electrons [38], which is larger than a direct dipole field.

In the present simple calculation, this contribution of the transferred field cannot be included.

Below T_{N2} , about half the In(3) sites do not feel any internal magnetic fields, while the In(4) sites feel nearly identical magnetic field. If the In(4) site exhibits field cancellation, its ν_4 line must split below T_{N2} . It is worth highlighting that the internal magnetic field of the In(3) site is mainly affected by the moment contribution from the Ce(1) site and some partial contribution from the Ce(2) site. On the other hand, the internal field at the In(4) site is influenced by the magnetic moments of the Ce(2) site only. This suggests that the wave vector of the Ce(2) site remains commensurate and that of the Ce(1) site changes into incommensurate in order to compensate the constant contribution, at the In(3) site, of the Ce(2) moments by modulation of the Ce(1) moments. If we do not consider the moment of the Ce(1) site, the commensurate order of the moment of the Ce(2) site produces double-peak structure for the ν_1 and ν_2 lines of the In(3) sites, even below T_{N2} , which was observed between T_{N1} and T_{N2} . This is inconsistent with the experimentally observed center line and broad satellite lines. Though most of the Ce(1) moment seems to have been screened by the Kondo effect, the existence of the tiny magnetic moment of the Ce(1) site is essential to explain the spectrum below T_{N2} . Since the transition at T_{N2} is clearly observed in thermodynamic quantities such as specific heat [18, 19, 21] and $1/T_1$ (described in the next section), the large magnetic moment of the Ce(2) site is responsible for the transition. This implies that the change of the wave vector at the Ce(2) site is essential, yielding a commensurate-to-commensurate transition: $(\frac{1}{2}, \frac{1}{2}, 0)$ to $(\frac{1}{2}, \frac{1}{2}, \frac{1}{2})$ or vice versa. Hence a wave vector of $(\frac{1}{2}, \frac{1}{2}, h)$ at the Ce(1) site with modulation in the k_z direction from $(\frac{1}{2}, \frac{1}{2}, 0)$ or $(\frac{1}{2}, \frac{1}{2}, \frac{1}{2})$ may account for the absence of any internal magnetic field at the In(3) site. This model was suggested before for the magnetic moment of the Ce(2) site by Kambe *et al.* [25]. However, in this case, the spectrum should be broadened for general h . Probably, h is modulated in the k_z direction in a way that brings about the cancellation of the internal magnetic field at half of the In(3) sites, although the exact h could not be determined within the present calculations. Further analysis beyond the simple dipole sum calculations is desired.

D. Spin-lattice relaxation rate $1/T_1$

Figure 7 shows the temperature dependence of the spin-lattice relaxation rate $1/T_1$ of the ν_4 line at the In(2) and In(3) sites. In both cases, two distinct transitions are observed at $T_{N1} \simeq 2.2$ K and $T_{N2} \simeq 2.0$ K. The observed relaxation curve can be fitted well to the theoretical formula expected for the ν_4 lines of $I = 9/2$ nuclei [39]. This result indicates that the longitudinal relaxation in $\text{Ce}_3\text{PtIn}_{11}$ is of magnetic origin and that there is almost no influence of the internal magnetic field even below T_{N1} , which is consistent with the conclusion that the internal

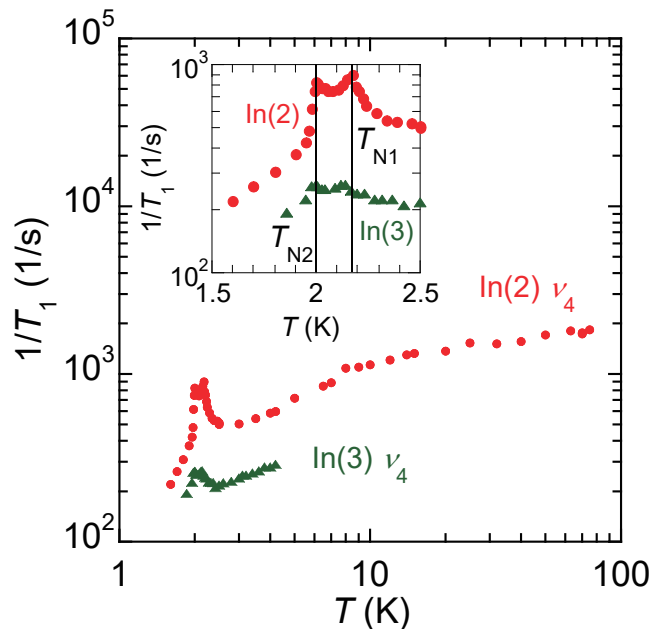


FIG. 7: Temperature dependence of the spin-lattice relaxation rate $1/T_1$ of $\text{Ce}_3\text{PtIn}_{11}$ for ν_4 lines of the In(2) and In(3) sites. Inset: magnified temperature dependence of $1/T_1$ between 1.5 and 2.5 K.

field is absent and small at the In(2) and In(3) sites, respectively. Here, it should be recalled that Kambe *et al.* pointed out that superconductivity is observed at the In sites that feel the internal magnetic fields [25].

IV. SUMMARY

NQR measurements were performed on the heavy-fermion superconductor $\text{Ce}_3\text{PtIn}_{11}$. The temperature dependencies of both $1/T_1$ and the NQR spectra revealed the occurrence of two successive magnetic transitions. Each inequivalent In site feels a single internal magnetic field between T_{N1} and T_{N2} , and the In(3) site feels two or three different internal magnetic fields below T_{N2} . Based on the NQR data we concluded that the magnetic wave vector is commensurate $(\frac{1}{2}, \frac{1}{2}, 0)$, or $(\frac{1}{2}, \frac{1}{2}, \frac{1}{2})$ with the magnetic moment parallel to the c axis between T_{N1} and T_{N2} . It was also revealed that the ordered magnetic moment at the Ce(2) site is about 25 times larger than that at the Ce(1) site. This indicates that the magnetic moment of the Ce(2) site plays a crucial role in the magnetism of $\text{Ce}_3\text{PtIn}_{11}$. The duality of the crystallographically inequivalent Ce sites is indeed realized in this compound. At T_{N2} , a complicated phase transition of commensurate to commensurate at the Ce(2) site and commensurate to incommensurate at the Ce(1) site is suggested. Further analysis beyond the simple dipolar model presented in this paper is desired. NQR studies performed at lower temperatures are required to conclude that the claimed coexistence of antiferromagnetism and superconductivity

in $\text{Ce}_3\text{PtIn}_{11}$ is an intrinsic property of this interesting material.

ACKNOWLEDGMENTS

The authors thank S. Kambe and T. Ohama for fruit-

ful discussions. This work was supported by JSPS KAKENHI Grant (No. 18K03505 and No. 19K14644). The work in Poland was supported by the National Science Centre (Poland) under Research Grant No. 2015/19/B/ST3/03158.

-
- [1] F. Steglich, J. Aarts, C. D. Bredl, W. Lieke, D. Meschede, W. Franz, and H. Schafer, *Phys. Rev. Lett.* **43**, 1892 (1979).
- [2] N. D. Mathur, F. M. Grosche, S. R. Julian, I. R. Walker, D. M. Freye, R. K. W. Haselwimmer, and G. G. Lonzarich, *Nature* **394**, 39 (1998).
- [3] C. Petrovic, P. G. Pagliuso, M. F. Hundley, R. Movshovich, J. L. Sarrao, J. D. Thompson, Z. Fisk, and P. Monthoux, *J. Phys.: Condens. Matter* **13**, L337 (2001).
- [4] H. Wang, J. Guo, E. D. Bauer, V. A. Sidorov, H. Zhao, J. Zhang, Y. Zhou, Z. Wang, S. Cai, K. Yang, A. Li, X. Li, Y. Li, P. Sun, Y.F. Yang, Q. Wu, T. Xiang, J. D. Thompson, and L. Sun, *Phys. Rev. B* **97**, 064514 (2018).
- [5] D. Das, D. Gnida, P. Wisniewski, and D. Kaczorowski, *PNAS* **116**, 20333 (2019).
- [6] Y. Kohori, Y. Yamato, Y. Iwamoto, T. Kohara, E. D. Bauer, M. B. Maple, and J. L. Sarrao, *Phys. Rev. B* **64**, 134526 (2001).
- [7] H. A. Ladovan, N. A. Fortune, T. P. Murphy, S. T. Hannahs, E. C. Palm, S. W. Tozer, and D. Hall, *Nature* **425**, 51 (2003).
- [8] A. Bianchi, R. Movshovich, C. Capan, P. G. Pagliuso, and J. L. Sarrao, *Phys. Rev. Lett.* **91**, 187004 (2003).
- [9] Y. Yanase and M. Sigrist, *J. Phys. Soc. Jpn.* **78**, 114715 (2009).
- [10] H. Hegger, C. Petrovic, E. G. Moshopoulou, M. F. Hundley, J. L. Sarrao, Z. Fisk, and J. D. Thompson, *Phys. Rev. Lett.* **84**, 4986 (2000).
- [11] S. Kawasaki, T. Mito, Y. Kawasaki, G.-q. Zheng, Y. Kitaoka, D. Aoki, Y. Haga, and Y. Onuki, *Phys. Rev. Lett.* **91**, 137001 (2003).
- [12] P. Monthoux and G. G. Lonzarich, *Phys. Rev. B* **63**, 054529 (2001).
- [13] D. Kaczorowski, A. P. Pikul, D. Gnida, and V. H. Tran, *Phys. Rev. Lett.* **103**, 027003 (2009); *ibid* **104**, 059702 (2010).
- [14] D. Kaczorowski, D. Gnida, A. P. Pikul, and V. H. Tran, *Solid State Commun.* **150**, 411 (2010).
- [15] H. Fukazawa, T. Okazaki, K. Hirayama, Y. Kohori, G. Chen, S. Ohara, I. Sakamoto, and T. Matusmoto, *J. Phys. Soc. Jpn.* **76**, 124703(2007).
- [16] H. Fukazawa, R. Nagashima, S. Shimatani, Y. Kohori, and D. Kaczorowski, *Phys. Rev. B* **86**, 094508 (2012).
- [17] A. Tursina, S. Nesterenko, Y. Seropegin, H. Noël, D. Kaczorowski, *J. Solid State Chem.* **200**, 7 (2013).
- [18] M. Kratochvílová, M. Dušek, K. Uhlířová, A. Rudajevová, J. Prokleška, B. Vondráčková, J. Custers, and V. Sechovský, *J. Cryst. Growth* **397**, 47 (2014).
- [19] J. Prokleška, M. Kratochvílová, K. Uhlířová, V. Sechovský, and J. Custers, *Phys. Rev. B* **92**, 161114(R) (2015).
- [20] M. Kratochvílová, J. Prokleška, K. Uhlířová, V. Tkáč, M. Dušek, V. Sechovský, and J. Custers, *Sci. Rep.* **5**, 15904 (2015).
- [21] D. Das, D. Gnida, L. Bochenek, A. Rudenko, M. Daszkiewicz, and D. Kaczorowski, *Sci. Rep.* **8**, 16703 (2018).
- [22] D. Das, D. Gnida, D. Kaczorowski, *Phys. Rev. B* **99**, 054425 (2019).
- [23] A. Benlagra, L. Fritz, and M. Vojta, *Phys. Rev. B* **84**, 075126 (2011).
- [24] S. Kambe, H. Sakai, Y. Tokunaga, R. E. Walstedt, M. Kratochvílová, K. Uhlířová, and J. Custers, *JPS Conf. Proc.* **29**, 011009 (2020).
- [25] S. Kambe, H. Sakai, Y. Tokunaga, R. E. Walstedt, M. Kratochvílová, K. Uhlířová, and J. Custers, *Phys. Rev. B* **101**, 081103(R) (2020).
- [26] N. J. Curro, P. C. Hammel, P. G. Pagliuso, J. L. Sarrao, J. D. Thompson, and Z. Fisk, *Phys. Rev. B* **62**, 6100(R) (2000).
- [27] W. Bao, P. G. Pagliuso, J. L. Sarrao, J. D. Thompson, Z. Fisk, J. W. Lynn, and R. W. Erwin, *Phys. Rev. B* **62**, R14621 (2000); **63**, 219901(E) (2001).
- [28] D. Das, J. Bławat, D. Gnida, and D. Kaczorowski (unpublished).
- [29] P. Blaha, K. Schwarz, F. Tran, R. Laskowski, G. K. H. Madsen, and L. D. Marks, *J. Chem. Phys.* **152**, 074101 (2020).
- [30] C. P. Slichter, *Principle of Magnetic Resonance*, 3rd edition, Springer Verlag (1989).
- [31] Because the natural abundance of ^{113}In is 4.3% and that of ^{115}In is 95.7%, the ^{113}In line intensities are quite low (see Fig. 3). The lines due to ^{113}In overlap with those of ^{115}In because the ratio of quadrupole moments is $^{113}Q/^{115}Q = 0.759/0.770$. However, they can be identified because of this ratio and the natural-abundance ratio.
- [32] W. Bao, P. G. Pagliuso, J. L. Sarrao, J. D. Thompson, Z. Fisk, and J. W. Lynn, *Phys. Rev. B* **64**, 020401(R) (2001).
- [33] Zh. M. Kurenbaeva, E. V. Murashova, Y. D. Seropegin, H. Noël, A. I. Tursina, *Intermetallics* **16**, 979 (2008).
- [34] H. Sakai, Y. Tokunaga, S. Kambe, H.-O. Lee, V. A. Sidorov, P. H. Tobash, F. Ronning, E. D. Bauer, and J. D. Thompson, *Phys. Rev. B* **83**, 140408(R) (2011).
- [35] M. Raba, E. Ressouche, N. Qureshi, C. V. Colin, V. Nassif, S. Ota, Y. Hirose, R. Settai, P. Rodiere, and I. Sheikin, *Phys. Rev. B* **95**, 161102(R) (2017).
- [36] N. Gauthier, D. Wermeille, N. Casati, H. Sakai, R. E. Baumbach, E. D. Bauer, and J. S. White, *Phys. Rev. B* **96**, 064414 (2017).

- [37] Strictly speaking, it is not impossible to explain the spectrum between T_{N1} and T_{N2} solely by the moment of the Ce(2) site if we consider transferred magnetic fields described below, which may be different at the In(3) and In(4) sites. However, it becomes more difficult to explain the spectrum below T_{N2} without the moment of the Ce(1) site.
- [38] N. J. Curro, *New J. Phys.* **8**, 173 (2006).
- [39] J. Chepin and J. H. Ross, *J. Phys.: Condens. Matter* **3**, 8103 (1991).